Czech B75 bentonite: mechanical properties and constitutive and numerical modelling

David Mašín

Charles University in Prague
team members: Czech Technical University, SURAO

BEACON
Bentonite Mechanical Evolution

BEACON kick-off meeting, Kaunas, Lithuania, 20. 5. 2017

This project receives funding from the Euratom research and training programme 2014-2018 under grant agreement No 745942

Outline

Černý vrch bentonite

- Bentonite from *Černý vrch deposit* (north-western region of the Czech Republic) selected as the primary buffer material in the Czech nuclear waste agency SURAO.

- *Calcium-magnesium bentonite* with a montmorillonite content of around 60% and initial water content in powder state of about 10%. Plastic limit 65%, liquid limit 229%, specific gravity 2.87.

Černý vrch bentonite

- Bentonite from *Černý vrch deposit* (north-western region of the Czech Republic) selected as the primary buffer material in the Czech nuclear waste agency SURAO.

- *Calcium-magnesium bentonite* with a montmorillonite content of around 60% and initial water content in powder state of about 10%. Plastic limit 65%, liquid limit 229%, specific gravity 2.87.

THM hypoplastic model for bentonites

- The model is based on *hypoplasticity* and it considers two structural levels, based on (*double structure* modelling concept by *Alonso et al., 1999*).

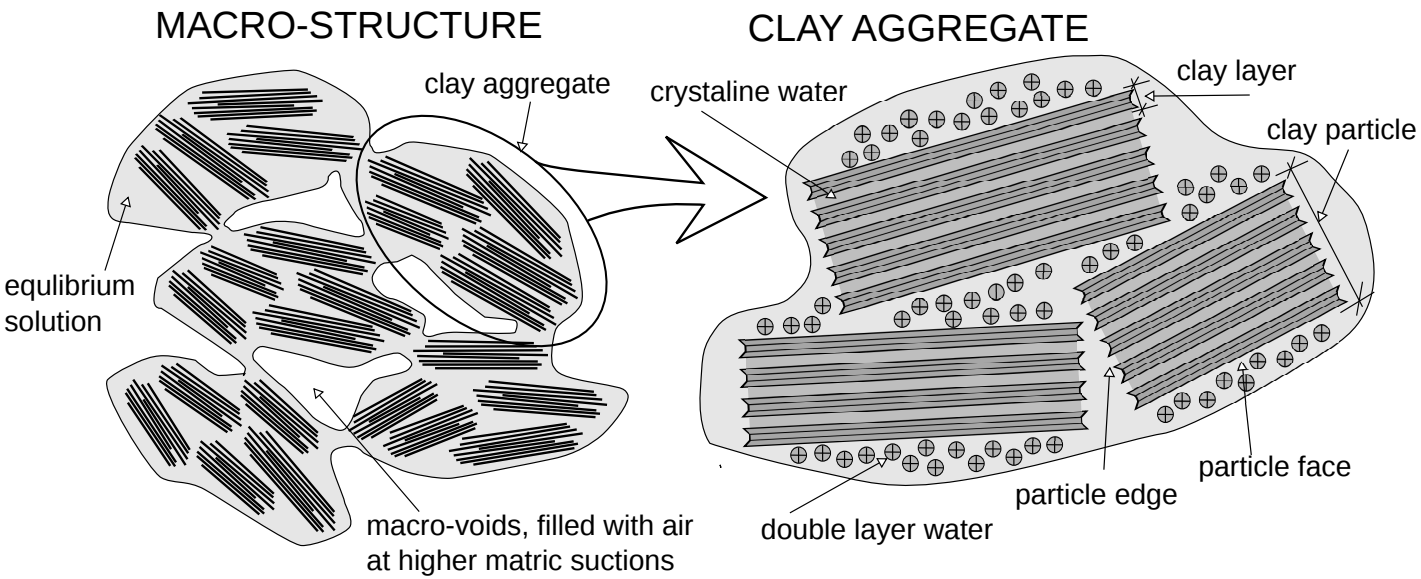

THM hypoplastic model for bentonites

- Separate *mechanical models* for macrostructure ($\mathbf{G}^M$) and microstructure ($\mathbf{G}^m$), defined using *effective stresses* $\boldsymbol{\sigma}^M$ and $\boldsymbol{\sigma}^m$.

$$\dot{\boldsymbol{\sigma}}^M = \mathbf{G}^M(\boldsymbol{\sigma}^M, \boldsymbol{q}^M, \dot{\boldsymbol{\epsilon}}^M) \quad \text{with} \quad \boldsymbol{\sigma}^M = \boldsymbol{\sigma}^{net} - \mathbf{1}s\chi^M$$
$$\dot{\boldsymbol{\sigma}}^m = \mathbf{G}^m(\boldsymbol{\sigma}^m, \boldsymbol{q}^m, \dot{\boldsymbol{\epsilon}}^m) \quad \text{with} \quad \boldsymbol{\sigma}^m = \boldsymbol{\sigma}^{net} - \mathbf{1}s\chi^m$$

- Two *water retention models* ($\mathbf{H}^M$ and $\mathbf{H}^m$) using micro- and macrostructural S_r.

$$\dot{S}_r^M = H^M(\dot{s}, s, \dot{\boldsymbol{\epsilon}}^M)$$
$$\dot{S}_r^m = H^m(\dot{s}, s, \dot{\boldsymbol{\epsilon}}^m)$$

THM hypoplastic model for bentonites

- Separate *mechanical models* for macrostructure ($\mathbf{G}^M$) and microstructure ($\mathbf{G}^m$), defined using *effective stresses* $\boldsymbol{\sigma}^M$ and $\boldsymbol{\sigma}^m$.

$$\dot{\boldsymbol{\sigma}}^M = \mathbf{G}^M(\boldsymbol{\sigma}^M, \boldsymbol{q}^M, \dot{\epsilon}^M) \quad \text{with} \quad \boldsymbol{\sigma}^M = \boldsymbol{\sigma}^{net} - \mathbf{1}s\chi^M$$
$$\dot{\boldsymbol{\sigma}}^m = \mathbf{G}^m(\boldsymbol{\sigma}^m, \boldsymbol{q}^m, \dot{\epsilon}^m) \quad \text{with} \quad \boldsymbol{\sigma}^m = \boldsymbol{\sigma}^{net} - \mathbf{1}s\chi^m$$

- Two *water retention models* ($\mathbf{H}^M$ and $\mathbf{H}^m$) using micro- and macrostructural S_r.

$$\dot{S}_r^M = H^M(\dot{s}, s, \dot{\epsilon}^M)$$
$$\dot{S}_r^m = H^m(\dot{s}, s, \dot{\epsilon}^m)$$

THM hypoplastic model for bentonites

- Separate *mechanical models* for macrostructure ($\mathbf{G}^M$) and microstructure ($\mathbf{G}^m$), defined using *effective stresses* $\boldsymbol{\sigma}^M$ and $\boldsymbol{\sigma}^m$.

$$\dot{\boldsymbol{\sigma}}^M = \mathbf{G}^M(\boldsymbol{\sigma}^M, \boldsymbol{q}^M, \dot{\boldsymbol{\epsilon}}^M) \quad \text{with} \quad \boldsymbol{\sigma}^M = \boldsymbol{\sigma}^{net} - \mathbf{1}s\chi^M$$
$$\dot{\boldsymbol{\sigma}}^m = \mathbf{G}^m(\boldsymbol{\sigma}^m, \boldsymbol{q}^m, \dot{\boldsymbol{\epsilon}}^m) \quad \text{with} \quad \boldsymbol{\sigma}^m = \boldsymbol{\sigma}^{net} - \mathbf{1}s\chi^m$$

- Two *water retention models* ($\mathbf{H}^M$ and $\mathbf{H}^m$) using micro- and macrostructural S_r.

$$\dot{S}_r^M = H^M(\dot{s}, s, \dot{\boldsymbol{\epsilon}}^M)$$
$$\dot{S}_r^m = H^m(\dot{s}, s, \dot{\boldsymbol{\epsilon}}^m)$$

THM hypoplastic model for bentonites

- Separate *mechanical models* for macrostructure ($\mathbf{G}^M$) and microstructure ($\mathbf{G}^m$), defined using *effective stresses* $\boldsymbol{\sigma}^M$ and $\boldsymbol{\sigma}^m$.

$$\dot{\boldsymbol{\sigma}}^M = \mathbf{G}^M(\boldsymbol{\sigma}^M, \boldsymbol{q}^M, \dot{\boldsymbol{\epsilon}}^M) \quad \text{with} \quad \boldsymbol{\sigma}^M = \boldsymbol{\sigma}^{net} - \mathbf{1}s\chi^M$$

$$\dot{\boldsymbol{\sigma}}^m = \mathbf{G}^m(\boldsymbol{\sigma}^m, \boldsymbol{q}^m, \dot{\boldsymbol{\epsilon}}^m) \quad \text{with} \quad \boldsymbol{\sigma}^m = \boldsymbol{\sigma}^{net} - \mathbf{1}s\chi^m$$

- Two *water retention models* ($\mathbf{H}^M$ and $\mathbf{H}^m$) using micro- and macrostructural S_r.

$$\dot{S}_r^M = H^M(\dot{s}, s, \dot{\boldsymbol{\epsilon}}^M)$$

$$\dot{S}_r^m = H^m(\dot{s}, s, \dot{\boldsymbol{\epsilon}}^m)$$

- *Hydro-mechanical coupling*: Hydraulic strain measure S_r^M depends on mechanical quantity $\dot{\boldsymbol{\epsilon}}^M$. Mechanical response influenced by χ^M, which may depend on a hydraulic quantity S_r^M.

THM hypoplastic model for bentonites

Predictions of heating-cooling tests, MX-80 bentonite, data by Tang et al. (2008)

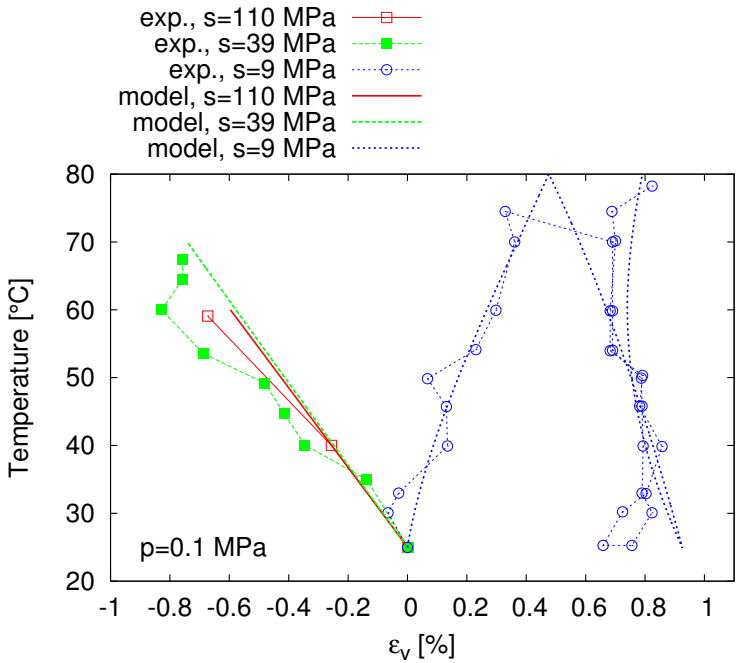

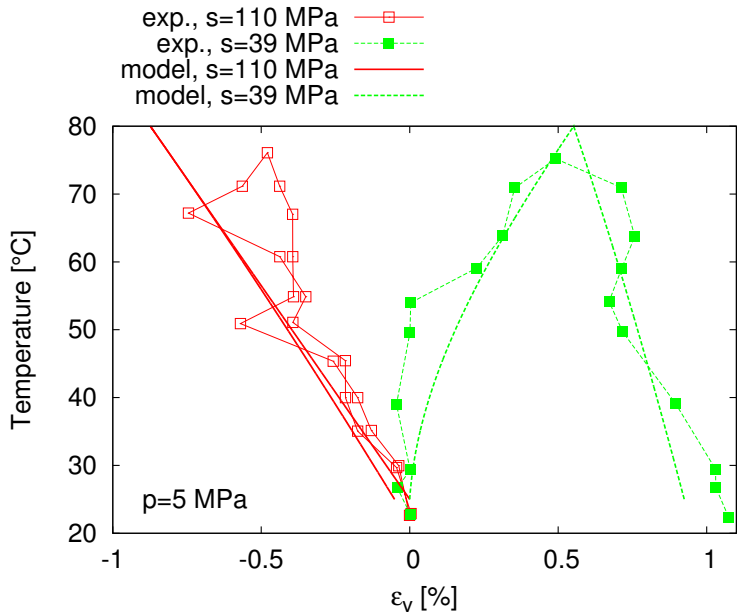

THM hypoplastic model for bentonites

Predictions of heating-cooling tests, MX-80 bentonite, data by Tang et al. (2008)

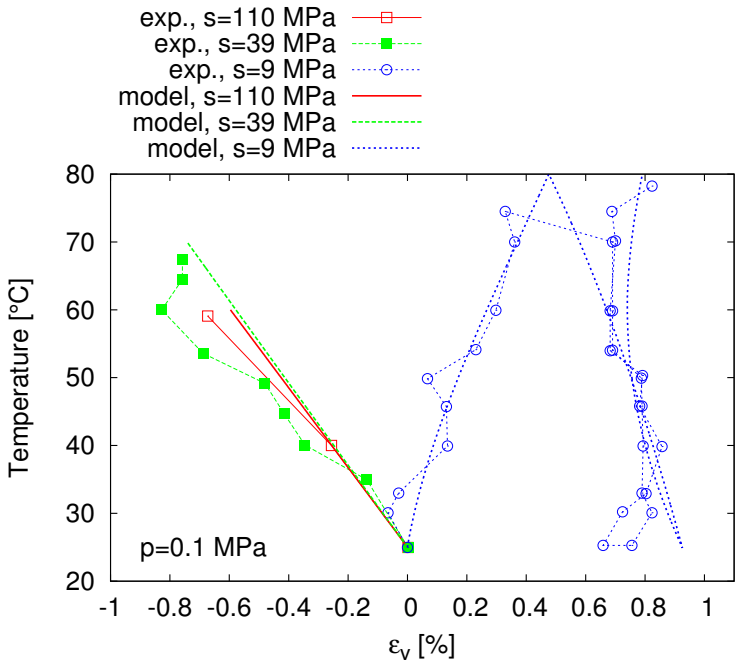

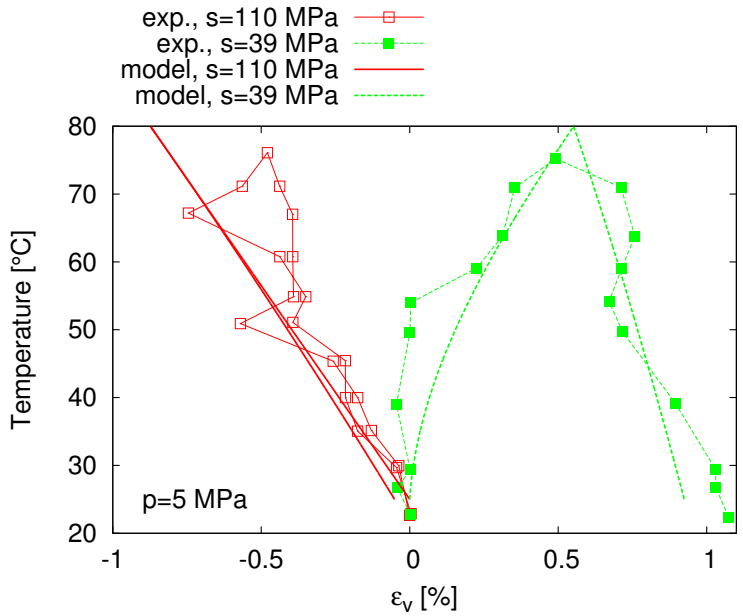

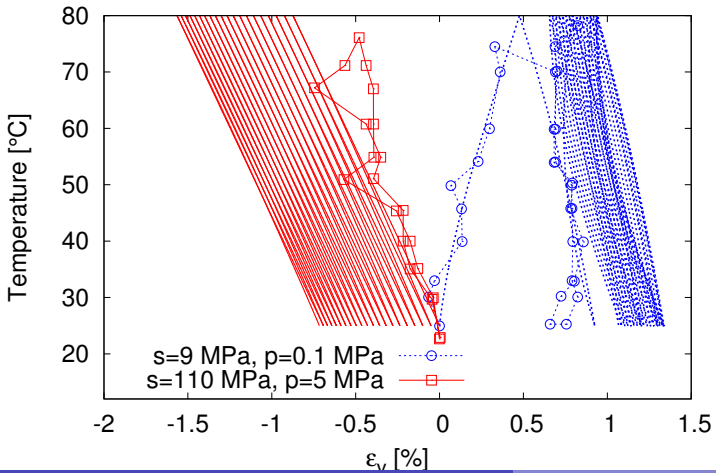

Cyclic heating-cooling test: no ratchetting problem as in standard hypoplasticity.

Microstructure of the Czech B75 bentonite

MIP testing

- *Mercury intrusion porosimetry* at samples with *two different initial dry densities* at suctions of *286.7 MPa, 38 MPa and 3.29 MPa*.
- Freeze-dried samples under mercury pressures between 0.01 MPa (0.1 mm pore radius) and 400 MPa (1.5 nm pore radius).

Microstructure of the Czech B75 bentonite

MIP testing

- *Mercury intrusion porosimetry* at samples with *two different initial dry densities* at suctions of *286.7 MPa, 38 MPa and 3.29 MPa*.
- Freeze-dried samples under mercury pressures between 0.01 MPa (0.1 mm pore radius) and 400 MPa (1.5 nm pore radius).

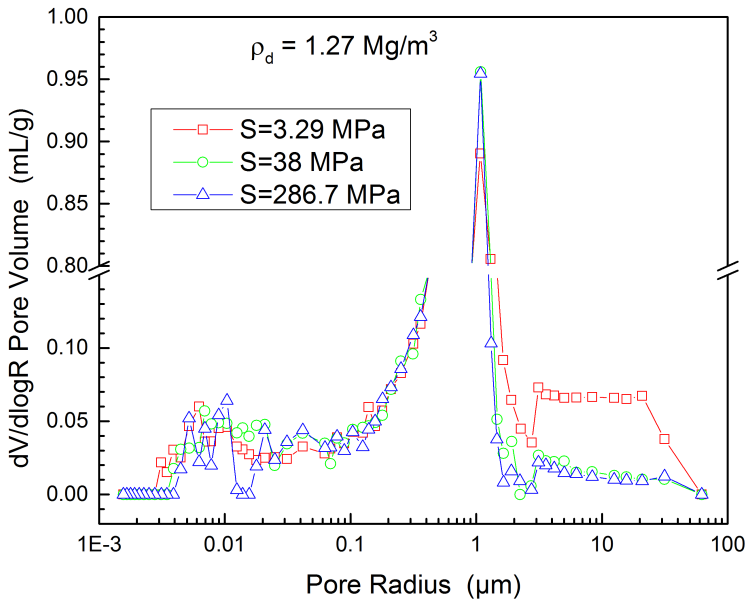

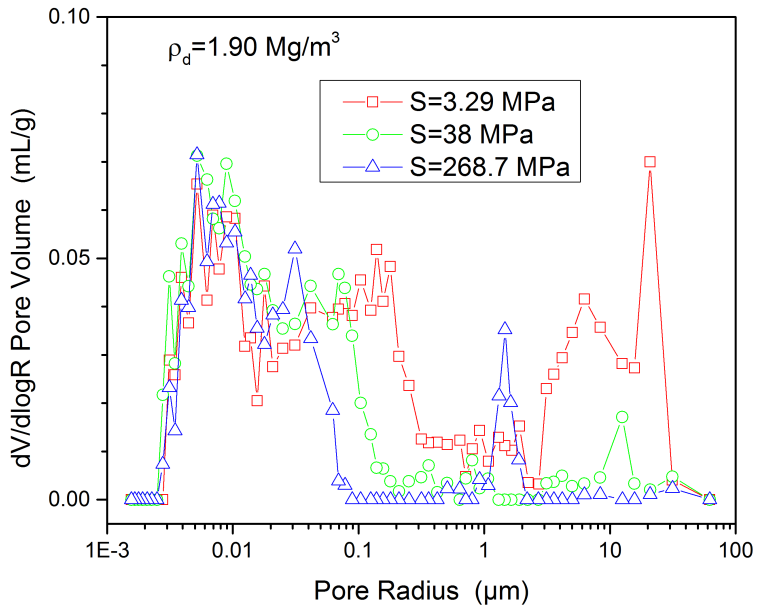

Microstructure of the Czech B75 bentonite

ESEM image analysis

- Microstructure studied using *environmental scanning electrone microscopy* (QUANTA 650 FEG).
- Samples equilibrated at a total suction of *287 MPa*.
- The vapour pressure imposed directly in the ESEM chamber, observation of the microstructure response to suction changes. Relative humidity varied between $10\% \rightarrow 97\% \rightarrow 10\%$.

Microstructure of the Czech B75 bentonite

ESEM image analysis

- Microstructure studied using *environmental scanning electrone microscopy* (QUANTA 650 FEG).
- Samples equilibrated at a total suction of *287 MPa*.
- The vapour pressure imposed directly in the ESEM chamber, observation of the microstructure response to suction changes. Relative humidity varied between $10\% \rightarrow 97\% \rightarrow 10\%$.

Microstructure of the Czech B75 bentonite

ESEM image analysis

- Microstructure studied using *environmental scanning electrone microscopy* (QUANTA 650 FEG).
- Samples equilibrated at a total suction of *287 MPa*.
- The vapour pressure imposed directly in the ESEM chamber, observation of the microstructure response to suction changes. Relative humidity varied between $10\% \rightarrow 97\% \rightarrow 10\%$.

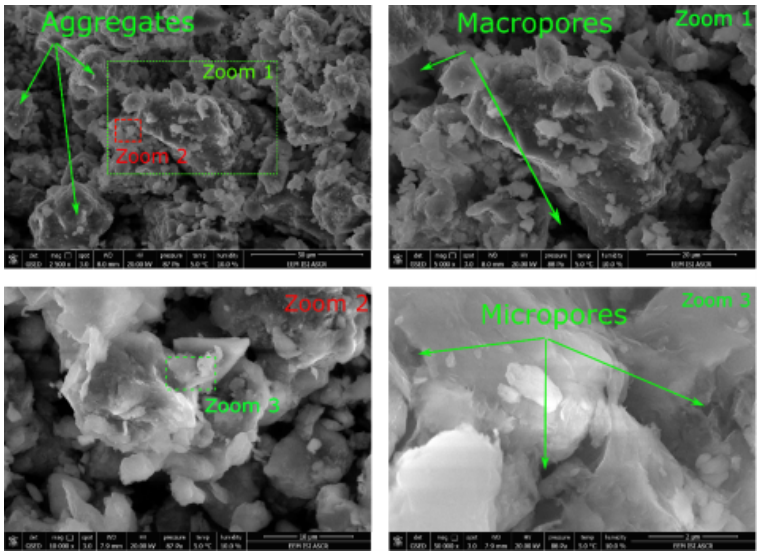

Microstructure of the Czech B75 bentonite

ESEM image analysis

- Movie of the aggregate swelling and shrinkage:

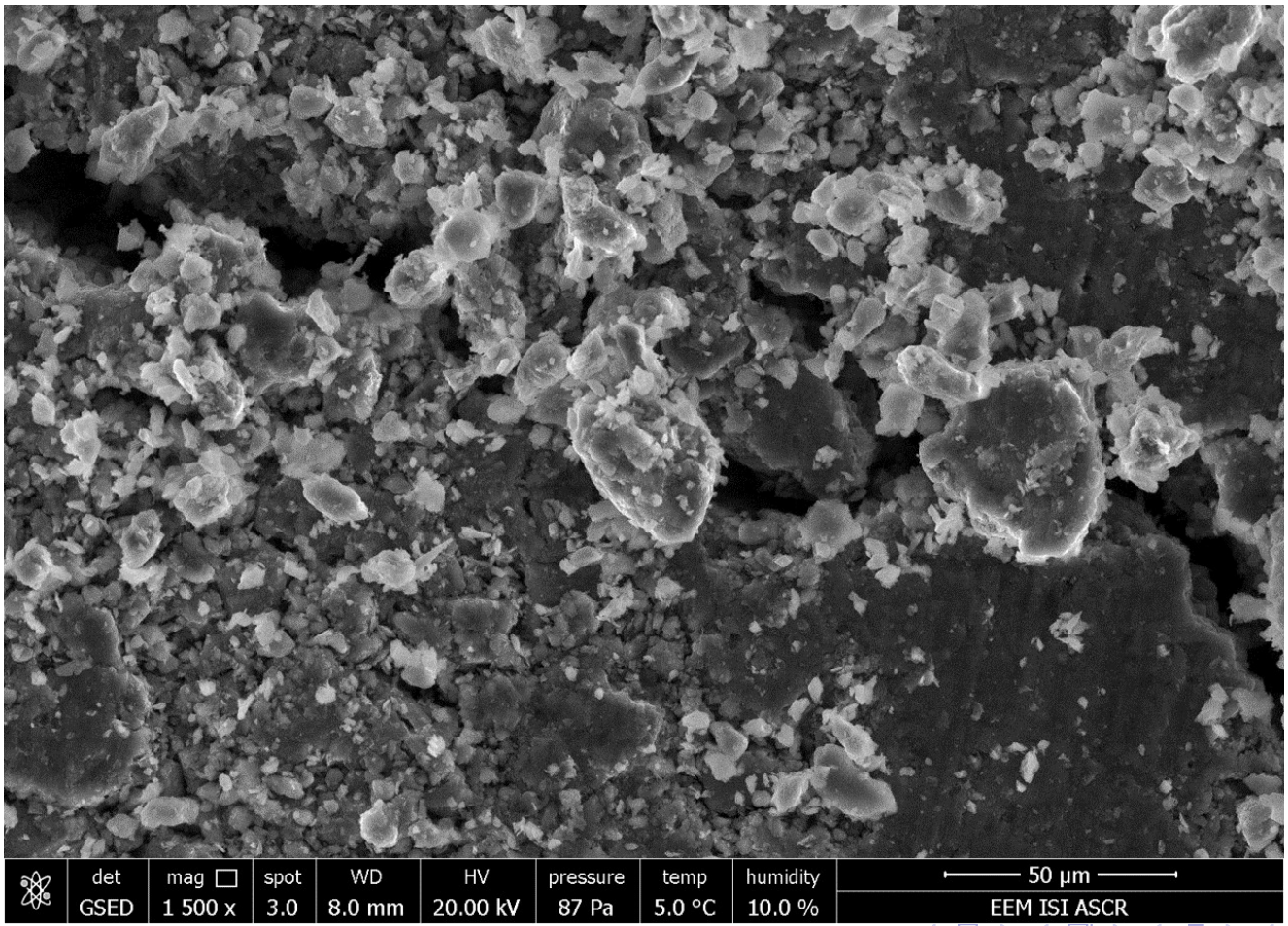

Microstructure of the Czech B75 bentonite

ESEM image analysis

- Quantification of microstructural swelling using *analysis of ESEM images*

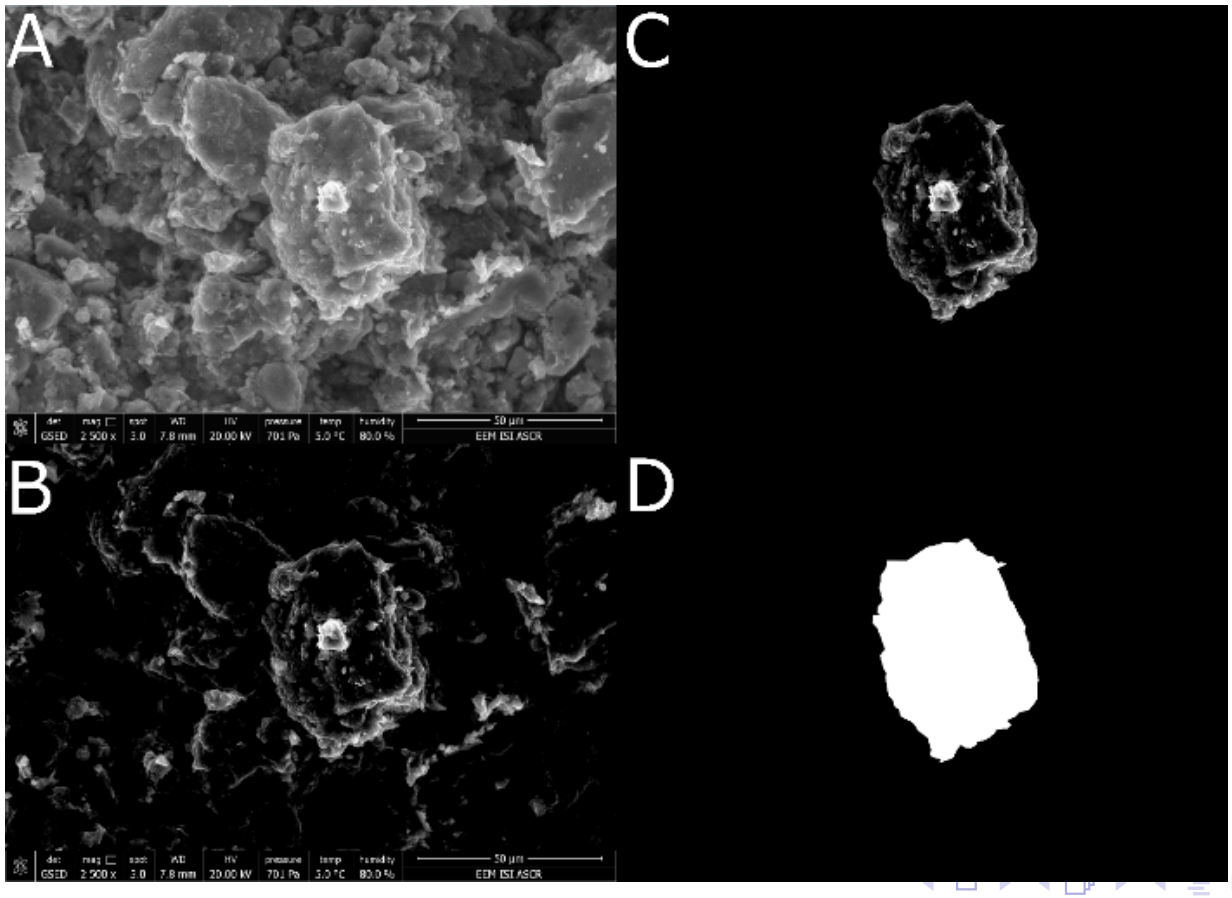

Microstructure of the Czech B75 bentonite

ESEM image analysis

- Volume changes of the aggregates *relatively small* until high relative humidities, where the aggregates increase in size significantly → *macropore volume change contributes to swelling*

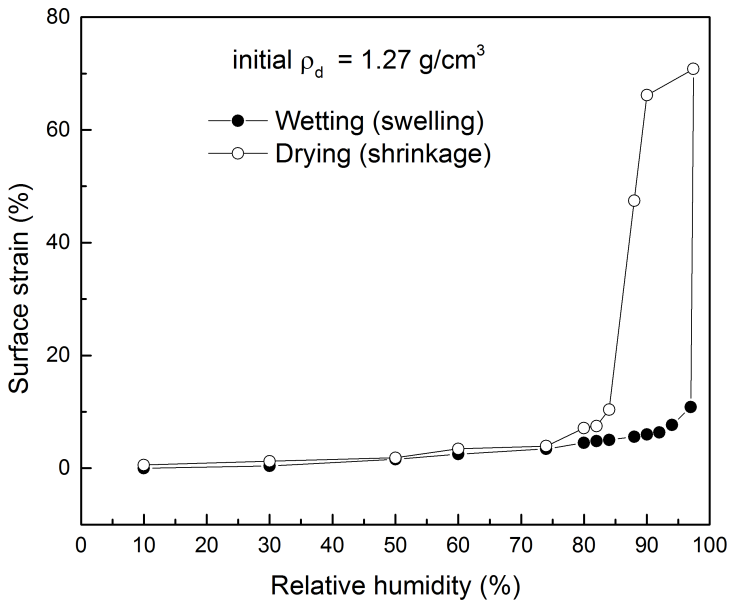

Microstructure of the Czech B75 bentonite

ESEM image analysis

- Volume changes of the aggregates *relatively small* until high relative humidities, where the aggregates increase in size significantly → *macropore volume change contributes to swelling*

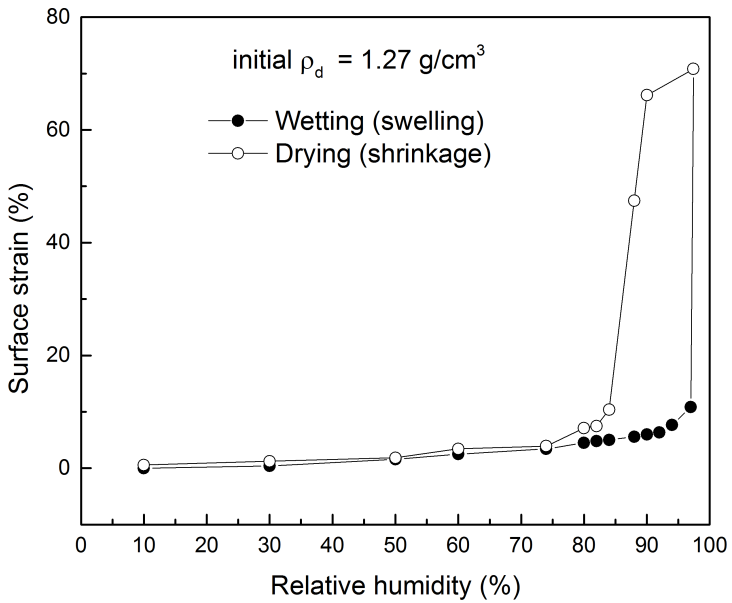

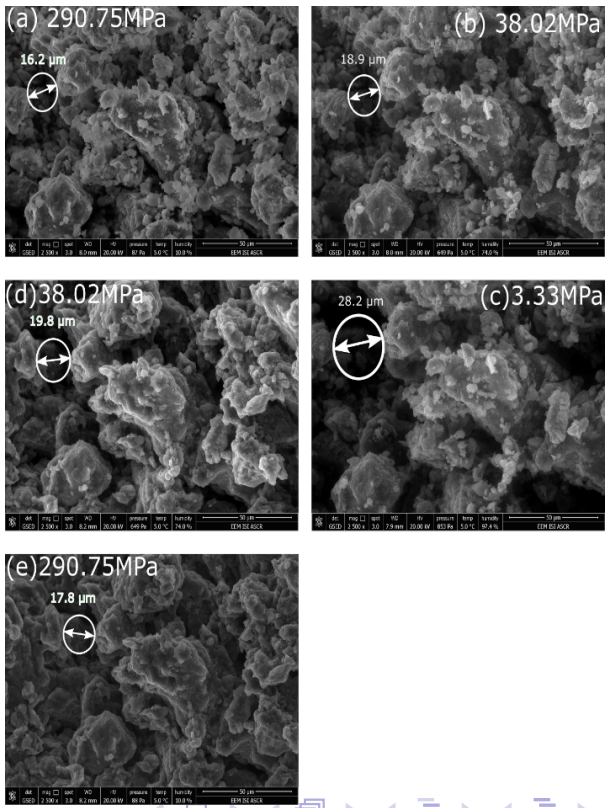

Hypoplastic model calibration

- Hypoplastic model calibrated using *free-swelling water retention tests*, *oedometric swelling under constant load tests* and *swellling pressure tests*

Hypoplastic model calibration

- Hypoplastic model calibrated using *free-swelling water retention tests*, *oedometric swelling under constant load tests* and *swellling pressure tests*

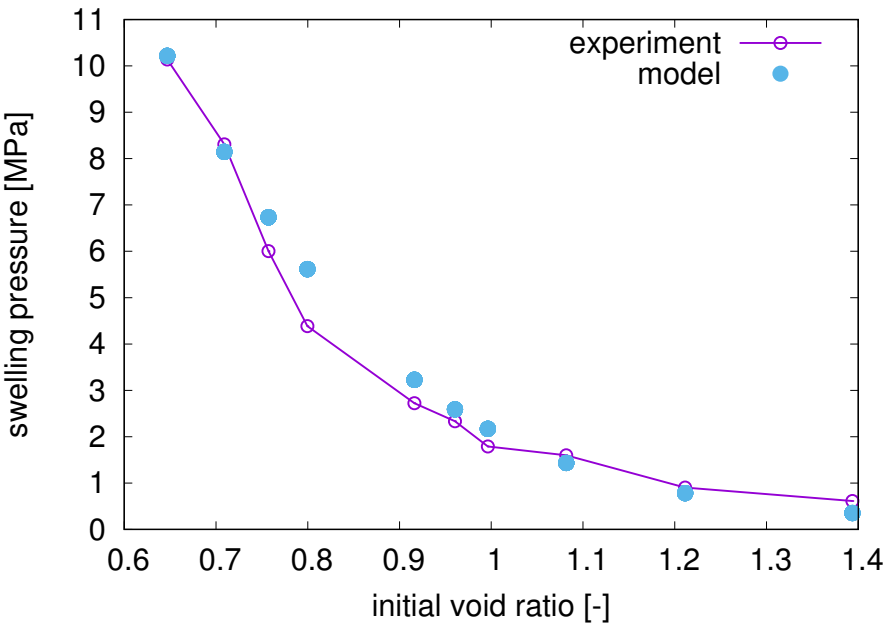

swelling pressure tests

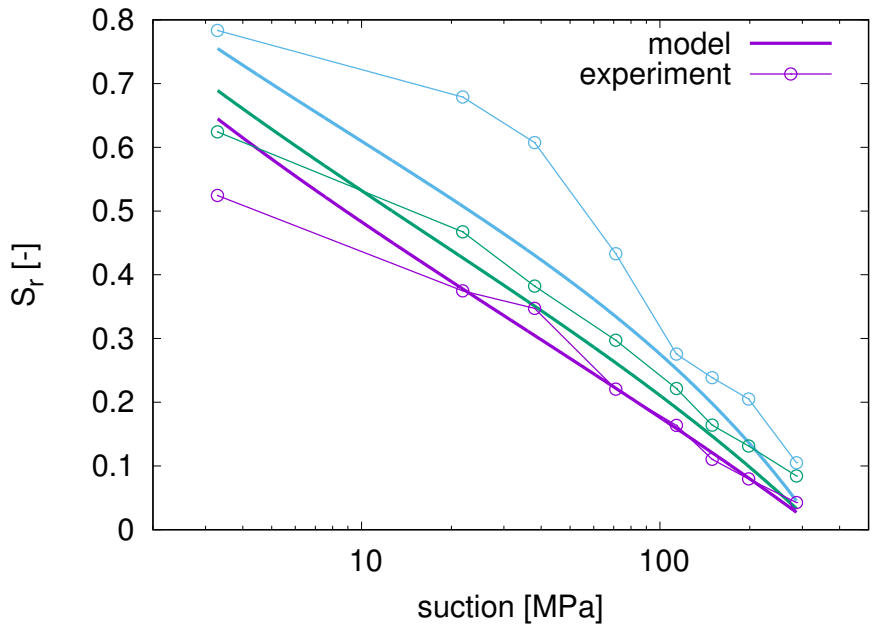

Water retention tests at various dry densities

Hypoplastic model calibration

- Oedometric and isotropic loading and unloading tests

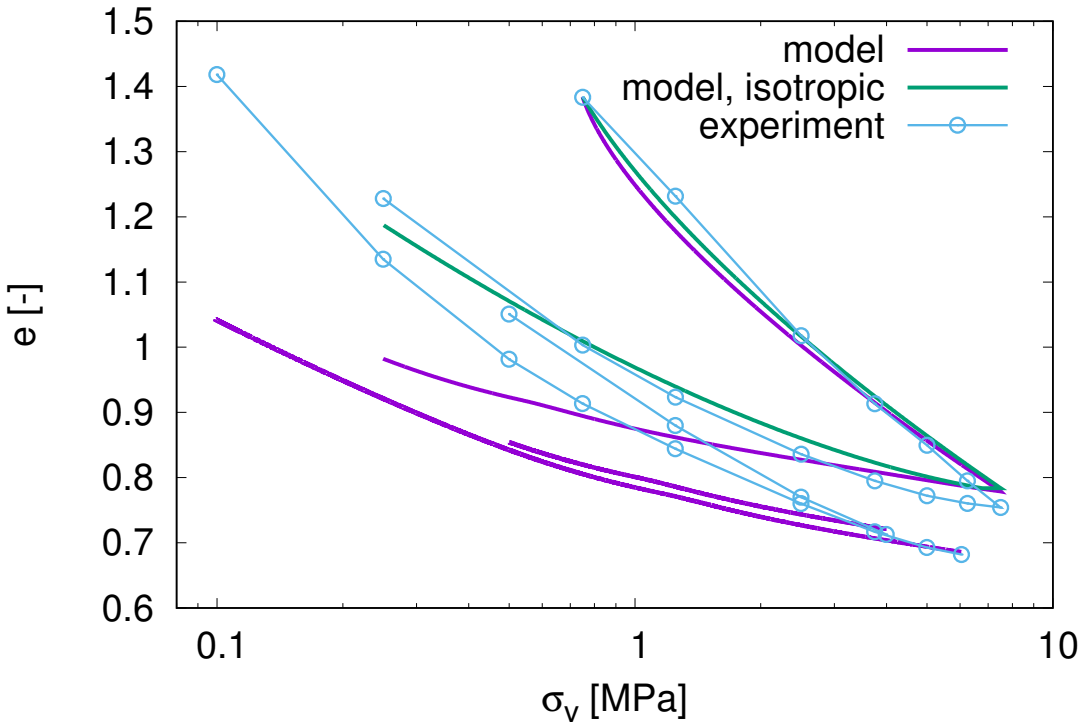

- $\Rightarrow$ Shortcoming of the double structure formulation - *microstructure deforms isotropically*, which is not the case in oedometric test

THM finite element simulations, software SIFEL

- Hypoplastic model implemented into an in-house coupled *THM finite element package SIFEL* (Czech Technical University).

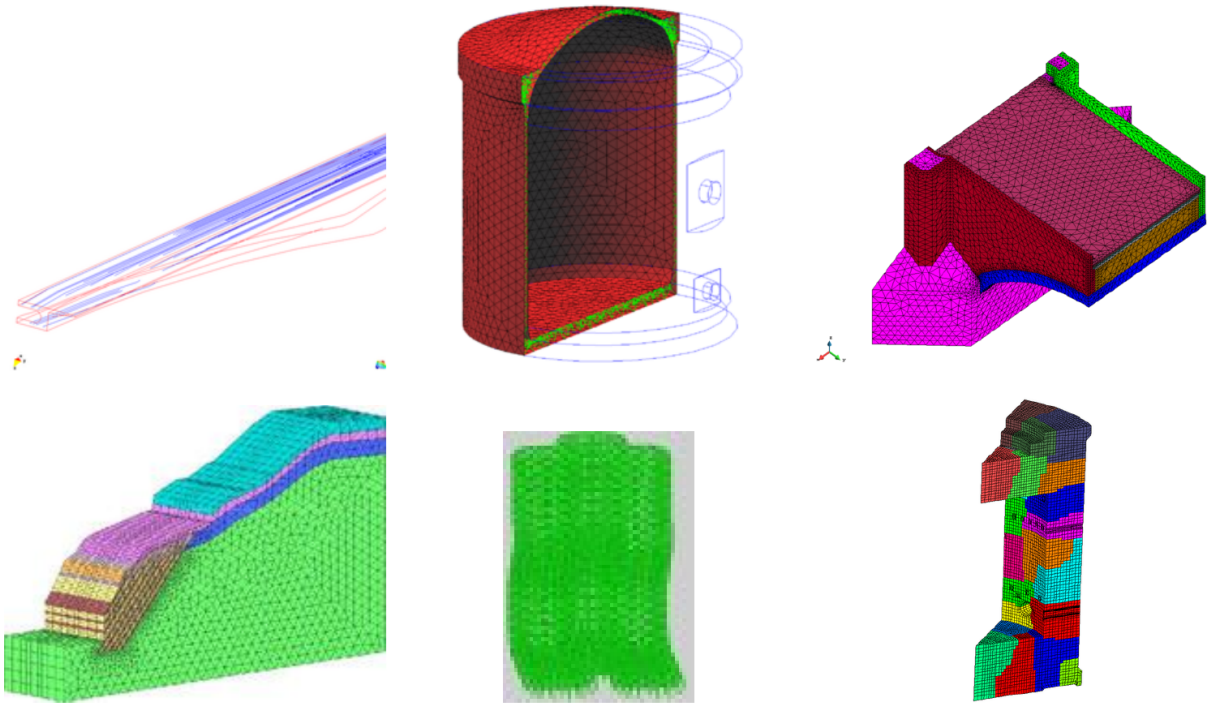

- Model calibrated using the element test data used for simulations of *constant water pressure gradient swelling pressure test* (Hausmannová, 2017)

THM finite element simulations, software SIFEL

- Hypoplastic model implemented into an in-house coupled *THM finite element package SIFEL* (Czech Technical University).

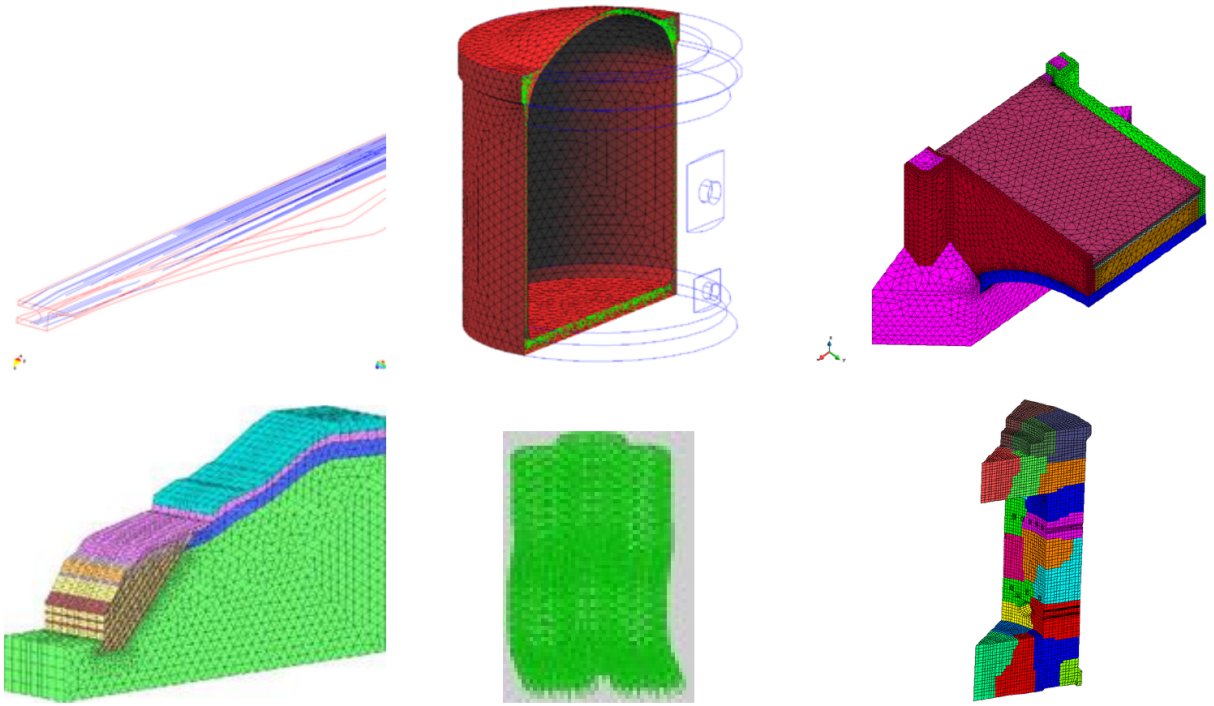

- Model calibrated using the element test data used for simulations of *constant water pressure gradient swelling pressure test* (Hausmannová, 2017)

THM finite element simulations, software SIFEL

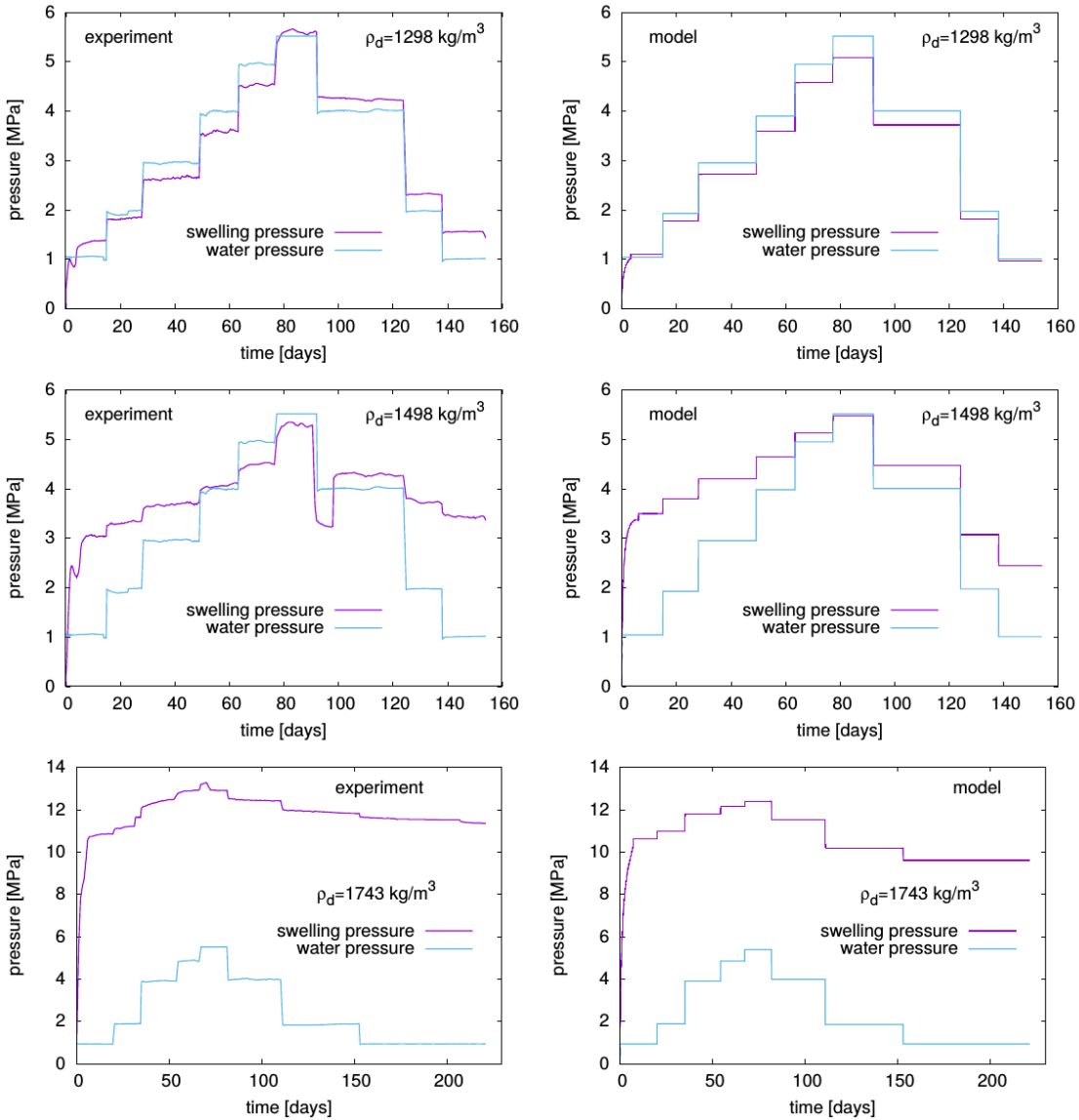

Czech Technical University in Prague

Faculty of Civil Engineering

Department of Mechanics

BEACON

Jaroslav Kruis, Tomáš Koudelka, Tomáš Krejčí

mass balance equations

$$\frac{\partial(n\,S_r\,\rho^w)}{\partial t} + \operatorname{div}\left(n\,S_r\,\rho^w\,\boldsymbol{v}^w\right) = \pm\dot{m} \quad \text{for liquid phase}$$

$$\frac{\partial\left((1-n)\,\rho^s\right)}{\partial t} + \operatorname{div}\left((1-n)\,\rho^s\,\dot{\boldsymbol{u}}\right) = 0 \quad \text{for solid phase}$$

Darcy's law

$$nS_r\left(\boldsymbol{v}^w - \dot{\boldsymbol{u}}\right) = \frac{k^{rw}\boldsymbol{k}_{\text{sat}}}{\mu^w}\left(-\operatorname{grad} p + \rho^w \boldsymbol{g}\right)$$

$$\left(\frac{\alpha-n}{K_g}S_r^2 + \frac{n\,S_r}{K_w}\right)\frac{\partial p}{\partial t} + \left(\frac{\alpha-n}{K_g}S_r\,p + n\right)\frac{\partial S_r}{\partial p}\frac{\partial p}{\partial t} +$$

$$+\alpha\,S_r\operatorname{div}\dot{\boldsymbol{u}} + \frac{1}{\rho^w}\operatorname{div}\left[\rho^w\frac{k^{rw}\boldsymbol{k}_{sat}}{\mu^w}\left(-\operatorname{grad} p + \rho^w\,\boldsymbol{g}\right)\right] = 0$$

strain-displacement relationship

$$\boldsymbol{\varepsilon} = \boldsymbol{\partial u}$$

constitutive equation

$$\boldsymbol{\sigma} = \mathcal{T}(\boldsymbol{\varepsilon}, \boldsymbol{q}) = \mathcal{T}(\boldsymbol{u}, \boldsymbol{q})$$

equilibrium condition

$$\mathrm{div}_x \boldsymbol{\sigma} + \boldsymbol{b} = \boldsymbol{0}$$

boundary conditions

$$\boldsymbol{u} = \bar{\boldsymbol{u}} \quad on\ \Gamma_u$$
$$\boldsymbol{\sigma}^{tot}\boldsymbol{n} = \bar{\boldsymbol{t}} \quad on\ \Gamma_t$$

Numerical solution (FEM)

approximation functions

$$\begin{aligned} \boldsymbol{u} &= \boldsymbol{N}_u \boldsymbol{d}_u \\ p &= \boldsymbol{N}_p \boldsymbol{d}_p \\ \boldsymbol{b} &= \boldsymbol{N}_u \hat{\boldsymbol{b}} \\ \bar{\boldsymbol{t}} &= \boldsymbol{N}_u \hat{\boldsymbol{t}} \end{aligned}$$

gradients and strains

$$\begin{aligned} \boldsymbol{\varepsilon} &= \boldsymbol{B}_u \boldsymbol{d}_u \\ \nabla p &= \boldsymbol{B}_p \boldsymbol{d}_p \end{aligned}$$

$$\begin{pmatrix} \mathbf{0} & \mathbf{0} \\ \boldsymbol{C}_{pu} & \boldsymbol{C}_{pp} \end{pmatrix} \begin{pmatrix} \dot{\boldsymbol{d}}_u \\ \dot{\boldsymbol{d}}_p \end{pmatrix} + \begin{pmatrix} \boldsymbol{K}_{uu} & \boldsymbol{K}_{up} \\ \mathbf{0} & \boldsymbol{K}_{pp} \end{pmatrix} \begin{pmatrix} \boldsymbol{d}_u \\ \boldsymbol{d}_p \end{pmatrix} = \begin{pmatrix} \boldsymbol{f}_u \\ \boldsymbol{f}_p \end{pmatrix}$$

the stiffness matrix

$$\boldsymbol{K}_{uu} = \int_\Omega \boldsymbol{B}_u^{\mathrm{T}} \boldsymbol{D} \boldsymbol{B}_u \, \mathrm{d}\Omega$$

the permeability matrix

$$\boldsymbol{K}_{pp} = \int_\Omega \boldsymbol{B}_p^{\mathrm{T}} \frac{k^{rw} \boldsymbol{k}_{\mathrm{sat}}}{\mu^w} \boldsymbol{B}_p \, \mathrm{d}\Omega$$

the compressibility matrix

$$\boldsymbol{C}_{pp} = \int_\Omega \boldsymbol{N}_p^{\mathrm{T}} \left(\frac{\alpha - n}{K_g} S_r \left(S_r + \frac{\partial S_r}{\partial p} p \right) + n \left(\frac{\partial S_r}{\partial p} + \frac{S_r}{K_w} \right) \right) \boldsymbol{N}_p \, \mathrm{d}\Omega$$

the coupling matrices

$$\boldsymbol{K}_{up} = -\int_{\Omega} \boldsymbol{B}_u^{\mathrm{T}} \alpha S_r \boldsymbol{i}^{\mathrm{T}} \boldsymbol{N}_p \,\mathrm{d}\Omega$$

$$\boldsymbol{C}_{pu} = \int_{\Omega} \boldsymbol{N}_p^{\mathrm{T}} \alpha S_r \boldsymbol{i}^{\mathrm{T}} \boldsymbol{B}_u \,\mathrm{d}\Omega$$

the load vector

$$\boldsymbol{f}_u = \int_{\Omega} \boldsymbol{N}_u^{\mathrm{T}} \boldsymbol{N}_u \hat{\boldsymbol{b}} \,\mathrm{d}\Omega + \int_{\Gamma_t} \boldsymbol{N}_u^{\mathrm{T}} \boldsymbol{N}_u \hat{\boldsymbol{t}} \,\mathrm{d}\Gamma$$

the flux vector

$$\boldsymbol{f}_p = \int_{\Omega} (\nabla \boldsymbol{N}_p)^{\mathrm{T}} \frac{k^{rw} \boldsymbol{k}_{\mathrm{sat}}}{\mu^w} \rho \boldsymbol{g} \,\mathrm{d}\Omega - \int_{\Gamma_w} \boldsymbol{N}_u^{\mathrm{T}} \frac{\overline{q}^w}{\rho^w} \,\mathrm{d}\Gamma$$

SIFEL (mech.fsv.cvut.cz/∼sifel)

- GEFEL - mathematical tools, solvers (77 000)
- MEFEL - problems of mechanics (191 000)
- TRFEL - transport processes (146 000)
- METR - coupled problems mechanics-transport processes (35 000)

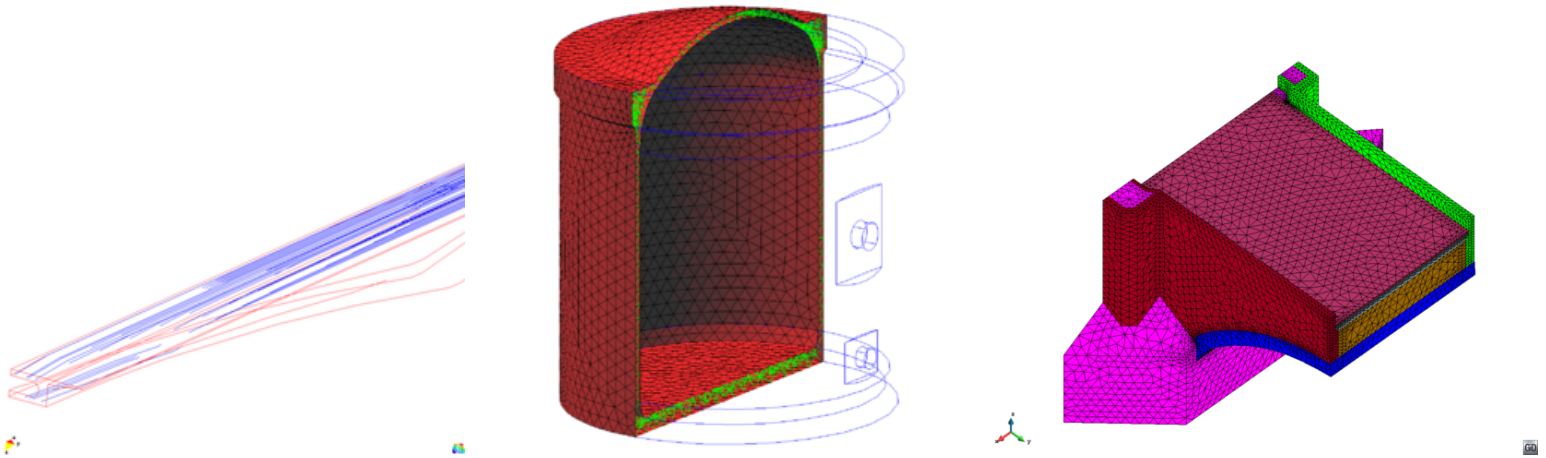

- 1D, 2D, 3D problems
- static–dynamic problems
- stationary–nonstationary problems
- problems with changing geometry